



The effect of electron-phonon interaction on the formation of reverse currents of p-n-junctions of silicon-based power semiconductor devices

Sergey V. Bulyarskiy

Institute of Nanotechnology of Microelectronics of the Russian Academy of Sciences, Moscow, Russia



ARTICLE INFO

Keywords:
 p-n-junction
 Current-voltage characteristic
 Generation
 Recombination
 Electron transition probability
 Electron-phonon interaction

ABSTRACT

The article represents the physical processes and mechanisms that accompany the work of the real p-n-junction. The nature of the reverse and forward currents of p-n-junctions is studied as the basis for the operation of these devices. The new model of recombination in space charge region of p-n-junction has been developed. This model made it possible to develop a new method for processing current-voltage characteristics and determining the parameters of recombination centers in semiconductor devices including electron-phonon interaction parameters. The probability of electronic transitions is calculated. It takes into account the electron-phonon interaction and explains the rapid build-up of reverse currents as the applied voltage increases. The mechanisms of formation of the reverse current of the p-n-junction were discussed and it was concluded that the current is determined by the generation with the participation of deep centers and electron-phonon interaction.

1. Introduction

The question about mechanisms of formation of the reverse current-voltage characteristic is one of the most complex. Basic formulas for current-voltage characteristics were developed in [1,2]. They were used in numerous scientific articles, for example [3–5] in the form:

$$j = j_s \left[\exp\left(\frac{eU}{mkT}\right) - 1 \right] \quad (1.1)$$

where j_s is reverse saturation current density; U is a voltage on the p-n-junction; k is the Boltzmann constant; e is electron charge; m is the ideality factor.

Ideality factor (m) has the meaning 1 in the Shockley diffusion theory [1] and 2 in the model generation and recombination in p-n-junctions [2]. The reverse saturation current density is associated with the parameter lifetime (τ) in the last model and it is in the form: $j_s = j_{s0}/\tau$. Classical reverse current does not depend on voltage. The dependence of the current on the voltage takes place in the so-called short-base diodes, when the base thickness is of the order of the diffusion length.

Scientific articles do not consider the problem that the ideality factor and the lifetime can depend on the voltage applied to the p-n-junction. Such an understanding of these values is not true, since the voltage value changes the flow of injected charge carriers. Ideality factor and the lifetime should change with a change in bias voltage too, because they depend on the injection. Numerous training courses and

lectures do not pay enough attention to this problem. However, the results of experimental research papers [3–7] have shown that the ideality factor does not remain constant [8–10], and the lifetime is not analyzed in such papers.

The theoretical reverse saturation current density is not dependent on applied voltage in the Shockley diffusion theory [1,11]. Experimental work shows that such a relationship takes place [3–6]. Some works leave this phenomenon without attention, and in others, the influence of applied voltage is explained by the Poole-Frenkel effect [12,13]. The coefficient of the Poole-Frenkel has a well-defined theoretical value and it must be calculated to prove the existence of this effect. This experimental coefficient may be more than theoretical. This is due to the influence of the electron-phonon interaction [14].

The mechanism of current flow can be determined by examining its dependence on temperature. Eq. (1.1) [1] predicts that the numerical value of the activation energy of the reverse current is close to the band gap of the semiconductor. The experimental value of the activation energy of this dependence is less than the theoretical one. This fact is determined by the process of generation of electrons and holes through the levels of deep centers. Reverse current was investigated in some articles describing the electrical properties of p-n-junctions [12,15–19]. The authors of [12] observed a monotonic increase in the reverse current of the diode, which with increasing temperature had the Arrhenius dependence form, with an activation energy from 0.10 to 0.16 eV. These amounts were dependent on the applied voltage. The behavior of current growth with temperature was explained by the

E-mail address: bulyar2954@mail.ru.

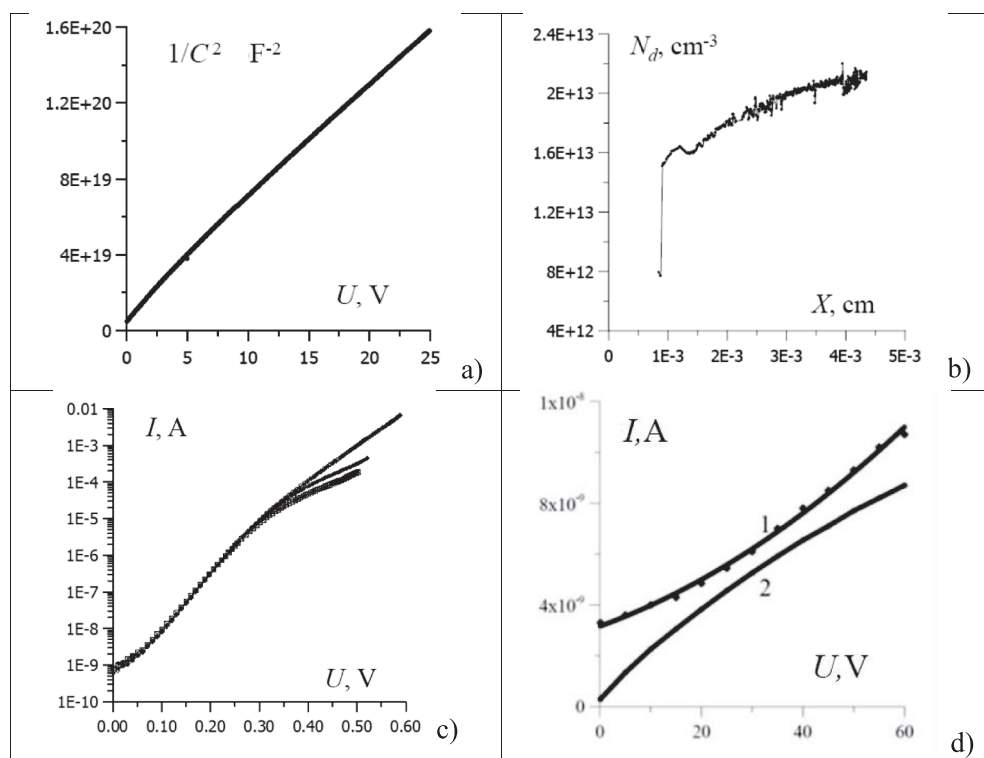


Fig. 1. Electrical characteristics of the diodes.

combined current transfer mechanism, which consists of hopping and thermo-activation conductivity with the participation of the Poole-Frenkel effect. The proposed model requires further study, since activation energy in an electric field is changed by 40%. This big change is not possible to explain only the Poole-Frenkel effect. The reverse current of silicon thyristors [19] monotonously increases with increasing applied voltage, and this dependence becomes exponential at high voltages. The experimental data from [19] allow us to estimate the activation energy for current growth with increasing p-n-junction temperature. It is equal to 0.64 eV, which is close to the middle of the forbidden zone of silicon and this value does not agree with theory [1]. The authors of [16] had suggested that the InSb-based diodes current-voltage characteristics are due to the interband tunneling model. However, the current is not dependent on temperature, if there is a tunnel process. The diode current of [16] grows with the activation law and has an activation energy of 0.09 eV. This does not satisfy the model that was proposed in [16]. The authors of [17] used Eq. (1.1) to describe their results. The experimental temperature dependences of the inverse current-voltage characteristics do not correspond to the theory [1]. Ideality factor is not equal to 2, it changes from 1.3 to 2. The theoretical model [17] that the authors chose did not agree with experiment.

In this way, the following facts are experimentally observed:

1. The reverse current of the p-n-junction depends on the voltage. The increase in current cannot be explained by the phenomenon of breakdown of the p-n-junction.

2. Thus, from the classical point of view, the reverse current should increase with temperature exponentially with an activation energy close to the width of the forbidden zone (E_g). The experimental value of the activation energy, as a rule, is less, therefore, there is no classical mechanism in the studied structures. The temperature dependence of the reverse current p-n-junction is not consistent with the theoretical (1.1).

Exponential current has activation energy E_a , which satisfies the inequality $E_g < E_a < 0.5E_g$. Such activation energies are a characteristic of generation electrons and holes with the participation of

recombination levels [2].

Multiphoton processes play an important role in generation recombination processes [14,21–25]. Electron–phonon interactions give rise to temperature dependence for capture coefficients and to an increase in the thermal emission rate in strong electric fields. In particular, it has been shown experimentally [21–23] and theoretically [14,20,23–25] that in strong electric fields, the probability of these transitions increases exponentially as the square of the electric field strength. Thus, more accurate calculations of the parameters of optoelectronic and power semiconductor devices associated with generation, recombination, and tunneling processes involving deep centers will require information on the parameters of the electron–phonon interactions which characterize a given electronic transition.

The theory has found practical application mainly for the single-coordinate model [14,21,23–25]. This model imposes rather rigid requirements on the character of the oscillations in the system and requires verification in each individual case. Degeneracy of the electronic states of a crystal with an impurity center causes the adiabatic approximation to fail and gives rise to vibrational mixing of the electronic levels. In this case, the single-coordinate model may not be suitable for calculating the field dependence.

In this paper, the probability of electronic transitions is calculated. It takes into account the electron–phonon interaction and explains the rapid build-up of reverse currents as the applied voltage increases. Methods for determining the parameters of recombination centers and electron–phonon interaction had been developed in this work and the reverse currents were calculated. This dependence agrees well with calculations that are made with allowance for electron–phonon interaction. The parameters of this interaction were found experimentally.

2. Experimental results

We used PIN-diodes with a 0.6 cm² working surface as convertors. The substrates of high quality monocrystalline silicon of the 100 KEF-4400 (1 1 1) brand (*n*-type silicon doped with phosphorous) were used as the initial material for the creation of PIN-diodes. The density of the

dislocations is less than 100 cm^{-2} according to the technical specifications for the wafers of this brand. The diode was manufactured according to the basic planar technology of diffusion structure. Defect's gettering was included in the process.

Diodes in the amount of 20 copies were manufactured and investigated. Measurements of their electrical properties were well reproduced. Typical characteristics of experimental samples are shown in Fig. 1.

Capacitance-voltage characteristics in coordinates $C^{-2} = f(U)$ are close to linear (Fig. 1a). This fact indicates a uniform distribution of impurities in the n-type quasi-neutral region. The calculation of the electron concentration (Fig. 1b), made on the basis of the capacitance-voltage characteristics, confirms this result. The forward current-voltage characteristics of 10 samples are shown in Fig. 1c. They coincide with each other and differ only in the magnitude of the series resistance of the contacts and the base of the diodes. The reverse current of the sample depends on the getter operation (Fig. 1d). There is more current without gettering. This is due to the fact that the internal gettering removes the vacancy-impurity complexes, which are of molecular nature.

a) Capacitance-voltage characteristics. b) The distribution of impurities in the quasi-neutral region of the n-type. c) Forward current-voltage characteristics (measurement results of 10 samples are superimposed on each other); e) Current-voltage characteristics at reverse bias: 1 is reverse current of samples without an internal gettering process; 2 is reverse current of samples in which the process of gettering defects has been incorporated into the technology.

The electron-phonon interaction is strong precisely for such defects and the generation currents with their participation depend on the electric field in the region of the space charge of the sample rather strongly. In the following paragraphs, the dependence of the ionization probability of defects in an electric field will be calculated and the calculation of the parameters of the electron-phonon interaction from current-voltage characteristics will be shown.

3. The parameters of the recombination centers which was determined by capacitive methods

Several authors, including [26], were developed the method of thermally stimulated capacity. Processing the results of measurements made by this method allows dividing the processes into components [27]. This work was developed later for multiple charged centers [28]. The dependence of the derivative of the thermally stimulated capacitance is shown in the Fig. 2a.

The derivative of the thermally stimulated capacitance is [27]:

$$\frac{\partial C}{\partial T} = A \left(\frac{T}{T_m} \right)^2 \exp \left[\frac{E_T}{k} \left(\frac{1}{T_m} - \frac{1}{T} \right) \right] \exp \left\{ 1 - \left(\frac{T}{T_m} \right)^2 \exp \left[\frac{E_T}{k} \left(\frac{1}{T_m} - \frac{1}{T} \right) \right] \right\} \quad (3.1)$$

where A is proportionality coefficient; T_m is the temperature of the maximum of the capacitance derivative, which determines the ionization of one of the recombination centers. This temperature is related to the capture rate constant and the activation energy by the formula:

$$c_n = \frac{\beta_T E_t}{k T_m^2 N_c} \exp \left(\frac{E_t}{k T_m} \right) \quad (3.2)$$

where β_T is the heating rate of the diode; N_c is the density of the electronic states of the conduction band.

The derivative was divided into separate components according to the method of work [27]. The thermal activation energy is only one parameter of Eq. (3.1). This equation is used. The activation energy varies in a certain energy range and the peak shape of the derivative of the thermally stimulated capacitance is calculated by Eq. (3.1). Energy

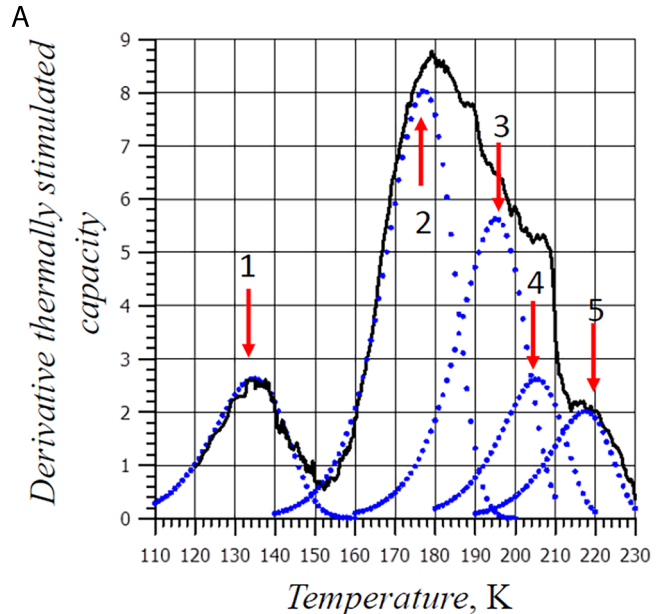


Fig. 2a. Dependence of the derivative of thermally stimulated capacitance from temperature. The points are the result of dividing the process into components by Eq. (3.1), with the following activation energy levels, eV: 1 – 0.16; 2 – 0.30; 3 – 0.38; 4 – 0.45; 5 – 0.52.

is accurate when the calculated and experimental curves coincide. Capture rate constant was calculated by (3.2). The concentration of recombination centers is determined directly from the curve of the thermally stimulated capacitance and is calculated as follows:

$$N_t = \frac{2C(T_{\min})N_d}{C(T_{\min}) - C(T_1)} \quad (3.3)$$

where T_{\min} is the temperature at which the derivative of the thermally stimulated capacity takes the minimum value in the region of high temperatures of the pick; T_1 is the same thing, but in the region of lower temperatures; N_d is the concentration of free charge carriers determined by the capacitive method (Fig. 1b). The results of the calculations are shown in Table 1. Spectra DLTS were processed by the classical method [29]. The emission rates are shown in Fig. 2b. The results of the calculations are shown in Table 1.

The results of TSC and DLTS are consistent with each other. The electron capture coefficients at the recombination centers are different, obtained by two different methods. We must take into account that the capture rate constant measurement of the emission rate by the DLTS method is higher. The capture rate constant is greater in this case. This difference will be discussed in the next paragraph.

Table 1

The parameters of the recombination centers, which were calculated from measurements of capacitance.

No	$E_t, \text{ eV}$	$C_n, \text{ cm}^3 \text{s}^{-1}$	$N_t * 10^{-11}, \text{ cm}^{-3}$
<i>Thermally stimulated capacity</i>			
1	0.16 ± 0.03	$(2.5 \pm 0.5) * 10^{-16}$	9
2	0.30 ± 0.03	$(5.0 \pm 0.5) * 10^{-12}$	10
3	0.38 ± 0.03	$(4.0 \pm 0.5) * 10^{-10}$	1
4	0.45 ± 0.03	$(2.0 \pm 0.5) * 10^{-7}$	3
5	0.53 ± 0.03	$(1.5 \pm 0.5) * 10^{-8}$	4
<i>Deep level transient spectroscopy (DLTS)</i>			
1	0.53 ± 0.03	$(7.0 \pm 0.5) * 10^{-7}$	5
2	0.45 ± 0.03	$(4.0 \pm 0.5) * 10^{-6}$	4
3	0.30 ± 0.03	$(4.0 \pm 0.5) * 10^{-10}$	9
4	0.16 ± 0.03	$(1.0 \pm 0.5) * 10^{-9}$	7

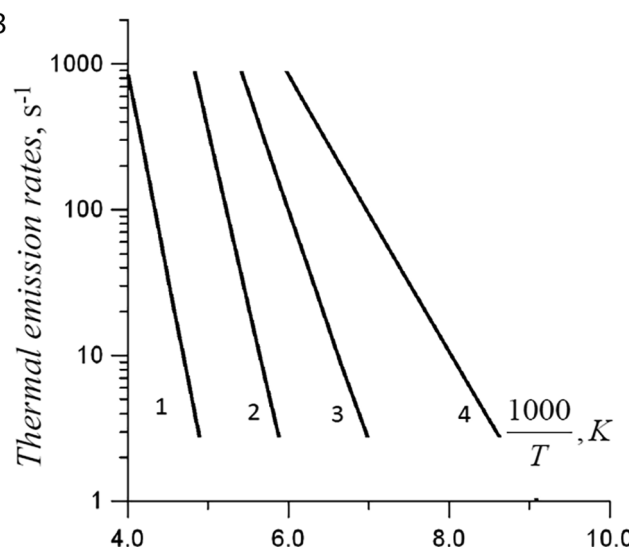


Fig. 2b. Thermal emission rates by DLTS. Activation energy levels, eV: 1 – 0.53; 2 – 0.45; 3 – 0.30; 4 – 0.16.

4. Recombination processes in the space charge region diodes

The forward currents of the initial part of the current-voltage characteristics of the p-n-junction are determined by a mechanism with recombination in the spatial domain as a rule [2]. The results of this work will be upgraded to facilitate the determination of the parameters of deep centers. The expressions for current-voltage characteristics of the diodes obtained in this work are based on the Shockley-Reed model [30]:

$$R(x) = \frac{c_n c_p N_t [n(x)p(x) - n_i^2]}{c_n [n(x) + n_i] + c_p [p(x) + p_i]} \quad (4.1)$$

where c_n, c_p are capture rate constant coefficients of electron and hole at a given center averaged over all states; $n_i = N_c \exp\left(-\frac{E_m}{kT}\right)$; $p_i = N_v \exp\left(-\frac{E_{tp}}{kT}\right)$; N_t is concentration of recombination's centers; E_t is the energy of the deep level; $E_m = E_C - E_t$; $E_{tp} = E_t - E_V$.

The magnitude of the recombination current is determined by the rates of four processes: the capture and emission of electrons and holes. The coordinate of the point where the recombination rate is at its maximum varies with the voltage at the p-n-junction. In particular, it may be on the edge of the space charge region (SCR). If the maximum of the recombination velocity shifts to the quasi-neutral region of the device, then this means a change in the recombination mechanism, when the approximations are not performed.

The concentration of free carriers in the space charge region can be obtained by multiplying the concentration of free carriers in the corresponding region by a Boltzmann factor, taking into account the influence of the p-n-junction electric field potential in $\text{SCR}(\phi(x))$. These concentrations are calculated by the formulas in a one-dimensional model:

$$\begin{aligned} n(x) &= n_n \exp\left(-\frac{e\phi(x)}{kT}\right), \\ p(x) &= p_p \exp\left(-\frac{e(V_d - U) - e\phi(x)}{kT}\right) \end{aligned} \quad (4.2)$$

where V_d is a diffusion potential; U is a voltage applied to the p-n-junction; n_n is a concentration of electrons in the n-region; p_p is a concentration of holes in the p region. The limits of the voltage change are chosen so that $\phi = 0$ if $x > x_n$ and $\phi = V_d - U$ if $x < x_p$.

The recombination rate (4.1) in the SCR is localized and represents a bell-shaped function with wings of an exponential type. The maximum of recombination is reached at the potential value.

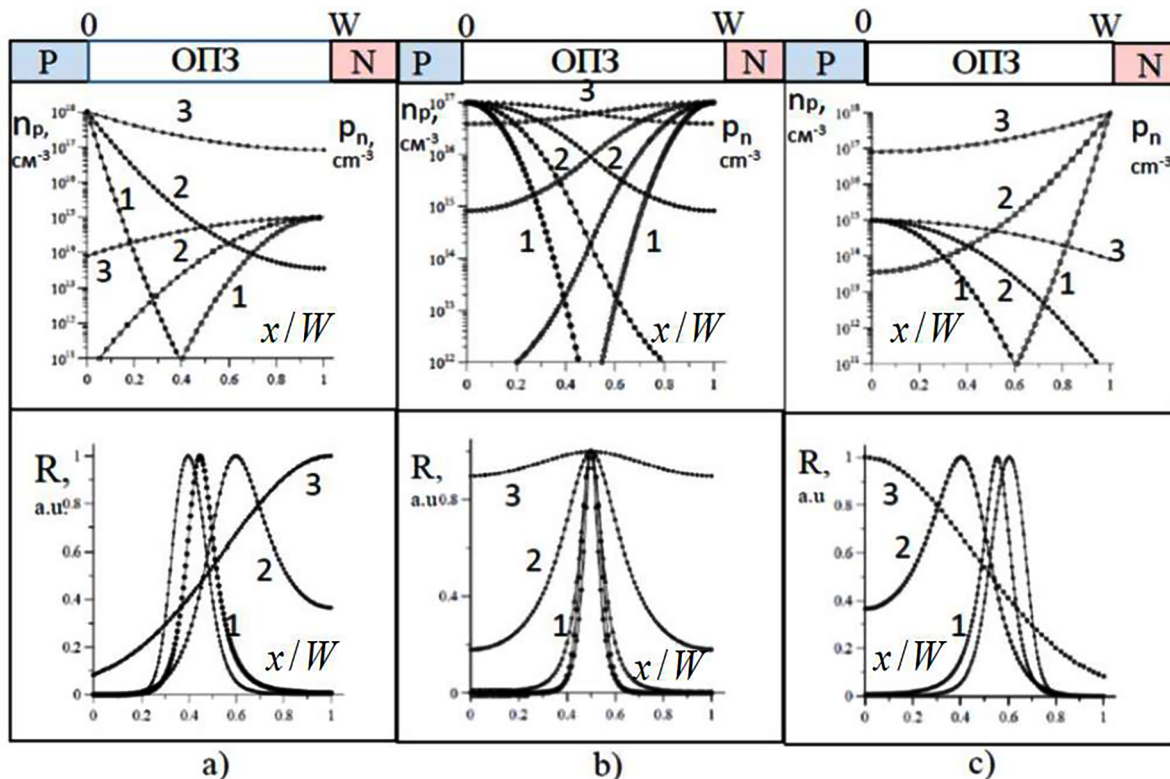


Fig. 3. Simulation of the minority carrier concentration and the recombination velocity in the space charge region using (4.2) and (4.4). In all cases there is: $c_n = c_p = 10^{-8} \text{ cm}^3 \text{ s}^{-1}$; direct bias voltage $U, \text{V}: 1 - 0.1 - 0.3; 2 - 0.5; 3 - 0.7$. The upper row represents the distribution of the concentration of injected charge carriers, the lower row recombination rate. a) Injection from the n-region – $N_D >> N_A$; b) injection from both areas $N_A = N_D$; c) injection from the p-region $N_D << N_A$.

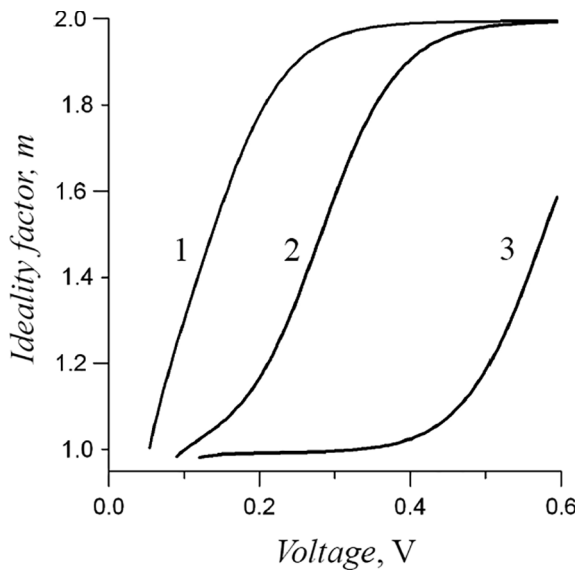


Fig. 4. Simulation of the ideality factor for the formulas (4.8) and (4.10) and the DLTS data of Table 1 for three recombination centers with activation energies, eV: 1 – 0.53 eV; 2 – 0.45; 3 – 0.30.

$$\phi_{\max} = \frac{e(V_d - U)}{2} + \frac{kT}{2e} \ln \left(\frac{c_n n_n}{c_p p_p} \right) \quad (4.3)$$

The recombination rate at this point is equal to:

$$R_{\max} = \frac{c_n c_p n_i^2 N_t \left[\exp\left(\frac{eU}{kT}\right) - 1 \right]}{2n_i \sqrt{c_n c_p} \exp\left(\frac{eU}{2kT}\right) + c_n n_i + c_p p_i} \quad (4.4)$$

The distribution of the recombination rate over the SCR is shown in Fig. 3 for various p-n-junctions. The shift of the maximum of this velocity always occurs to the edge of the less doped region. The voltage at the p-n-junction corresponds to the boundary when the maximum recombination rate is on the edge of the depleted region:

- When $\phi = 0$, $x = x_n$. This condition is realized when the p-region of the transition is doped more strongly. The voltage at which the maximum recombination rate is within the SCR is determined by the formula:

$$eU = eV_d + \frac{kT}{e} \ln \frac{c_n n_n}{c_p p_h} = E_g - \frac{kT}{e} \ln \frac{c_p N_c N_v}{c_n n_n^2}. \quad (4.5)$$

- When $\phi = e(V_d - U)$, $x = x_p$ n-region doping of the p-n-junction is stronger.

$$eU = eV_d + \frac{kT}{e} \ln \frac{c_p p_p}{c_n n_n} = E_g - \frac{kT}{e} \ln \frac{c_p N_c N_v}{c_n p_p^2}. \quad (4.6)$$

In a symmetric p-n-junction, in which the concentration of the doping is the same on both sides, the maximum recombination rate lies within the SCR up to voltages close to the diffusion potential.

The equation for the current-voltage characteristic can be obtained from the Eq. (4.4). We can calculate concentration of electrons and holes when the recombination rate reaches a maximum using the derivative of the Eq. (4.4). We get the concentration of injected charge carriers:

$$n = n_i \sqrt{\frac{c_p}{c_n}} \exp(eU/2kT), \quad p = n_i \sqrt{\frac{c_n}{c_p}} \exp(eU/2kT). \quad (4.7)$$

where it follows that [8,9]: $\int_{-x_p}^{x_n} R(x)dx \approx 2R_{\max} \Delta x = \frac{2kT}{eF} R_{\max}$, where F is the average field strength in the p-n-junction is equal to $F = \frac{w(U)}{e(V_d - U)}$.

We get for the current formula:

$$I_r(U) = eSw(U) \frac{c_n c_p n_i^2 N_t (e^{eU/kT} - 1)}{2n_i \sqrt{c_n c_p} e^{eU/2kT} + c_n n_i + c_p p_i} * \frac{2kT}{e(V_d - U)}. \quad (4.8)$$

If several deep centers are involved in the recombination process, the resulting current is the sum of the recombination currents through each center.

$$I_r = \sum_{m=1}^g \frac{eSw(U) c_{nm} c_{pm} n_i^2 (e^{eU/kT} - 1) N_{lm}}{2n_i \sqrt{c_{nm} c_{pm}} e^{eU/2kT} + c_{nm} n_{lm} + c_{pm} p_{lm}} * \frac{2kT}{e(V_d - U)}, \quad (4.9)$$

where $w(U)$ is the width of the SCR, g is the number of doubly charged recombination centers simultaneously participating in the recombination process.

Analysis of the expression (4.8) shows that the current-voltage characteristics change the slope at voltage, when the first term in the denominator (4.8) is equal to the sum of the other two. The current-voltage characteristic at low forward bias voltages varies according to the law: $\exp\left(\frac{eU}{kT}\right)$. Its slope decreases in the next section: $\exp\left(\frac{eU}{2kT}\right)$. These characteristic areas can be used to calculate the parameters of deep centers. However, the current-voltage characteristics depend on the voltage exponentially. They must be transformed before calculating the parameters of the recombination processes associated with individual deep centers.

The slope of the current-voltage characteristic is changed when the voltage at the p-n-junction grows. Therefore, the ideality factor m also changes. The magnitude of the ideality of a factor is determined by the formula, which we obtain from Eq. (1.1):

$$m = \frac{e}{kT} \left(\frac{d \ln I_r}{dU} \right)^{-1} = \frac{eI_r}{kT} \left(\frac{dI_r}{dU} \right)^{-1} \quad (4.10)$$

We substitute Eq. (4.8) into Eq. (4.10) and perform numerical simulations, while using the DLTS data of Table 1 for the three recombination centers (0.30, 0.45 and 0.53 eV). The simulation results are shown in Fig. 4.

The simulation results show that the ideality factor changes from 1 to 2 with a change in voltage at the p-n-junction. This is determined by the increase in the concentration of injected charge carriers in the depleted region and the change in recombination fluxes through deep centers.

5. Recombination spectroscopy. Reduced recombination Rate

Current-voltage characteristic, which is described by formulas (4.8) and (4.10) monotonously increases. An increase in current is determined by an exponential increase in the concentration of injected electrons and holes. Therefore, the slopes of the volt-ampere characteristic to segregate and identify the features of the experimental current – voltage characteristic is not simple. These features can be calculated by recombination spectroscopy [8-10]. Recombination spectroscopy is the method for converting experimental volt-ampere characteristics into curves that have certain characteristic features and allows them to calculate the parameters of deep centers.

The method of converting the current-voltage characteristic is based on the introduction of the superficial recombination rate. For the analysis of the current-voltage characteristics, a physical quantity is introduced, which is called the reduced recombination rate (R_{pr}) [8-10], which is determined by

$$R_{pr}(U) = \frac{I_r(U)}{eSw(U)n_i \left[\exp\left(\frac{qU}{2kT}\right) - 1 \right]} \frac{e(V_d - U)}{2kT} \quad (5.1)$$

The current-voltage characteristic in the recombination region in the depleted region is:

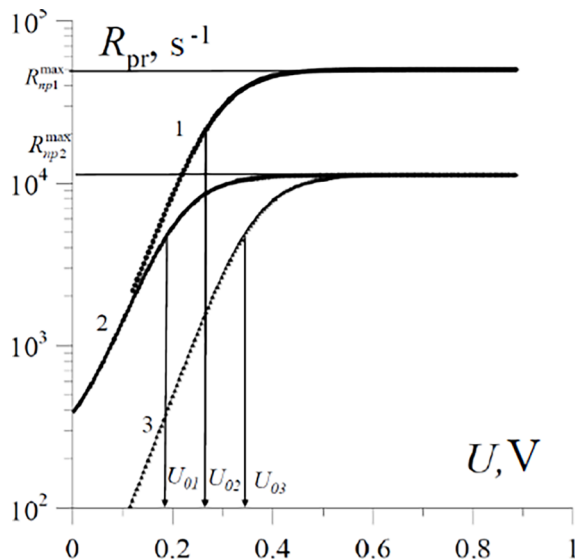


Fig. 5. Modeling the reduced recombination rate for deep centers with an activation energy of 0.4 eV for three ratios of recombination coefficients: c_n/c_p : 1 – 2 – 10; 2 – 10; 3 – 0.1.

$$I_r(U) = \frac{eSw(U)n_i}{\tau} \left[\exp\left(\frac{eU}{2kT}\right) - 1 \right]$$

where τ is the lifetime. This expression makes it possible to understand that the reduced recombination rate is a quantity that is the inverse of the lifetime.

The parameters of deep centers can be calculated if the recombination current is greater than the diffusion current. The reduced recombination rate is determined by the parameters of deep centers. Мы получаем формулу для этой величины, когда подставляем Eqs. (4.8) в (5.1)

$$R_{pr} = \frac{c_n c_p n_i N_t \left[\exp\left(\frac{eU}{2kT}\right) + 1 \right]}{2n_i \sqrt{c_n c_p} \exp\left(\frac{qU}{2kT}\right) + n_1 c_n + p_1 c_p} \quad (5.2)$$

Fig. 5 shows the dependence of the reduced recombination rate on voltage. The curve consists of two sections. The first section of Fig. 5 satisfies the inequality $2n_i \sqrt{c_n c_p} \exp\left(\frac{qU}{2kT}\right) > n_1 c_n + p_1 c_p$ and is described by the following dependency:

$$R_{pr} = c_p \left(\frac{m_p^*}{m_n^*} \right)^{3/4} N_t \exp\left(-\frac{E_g - E_t}{kT}\right) \exp(eU/2kT) \quad (5.3)$$

The second section of Fig. 5 satisfies the inequality $2n_i \sqrt{c_n c_p} \exp\left(\frac{qU}{2kT}\right) < n_1 c_n + p_1 c_p$, in addition, if the energy level of the deep center is located above or below the middle of the zone, then one term of two in the right-hand side of the inequality can be used. We believe that $n_1 c_n > p_1 c_p$, then:

$$R_{pr} = R_{pr}^{\max} = \sqrt{c_n c_p} N_t / 2 \quad (5.4)$$

The graph of the reduced recombination rate function consists of two straight lines. The first line is changed according to the law $\exp\left(\frac{eU}{2kT}\right)$ is linear in the coordinates $\ln(R_{pr}) = f(U)$ (Eq. (5.3)). The second line is parallel to voltage axis (Eq. (5.4)). Therefore, we can set a graph of the reduced recombination rate by one point on the plane, which is created by the axes (R_{pr}) and (U). This point is the intersection of lines, which are described by Eqs. (5.3) and (5.4). This property of the graph of the reduced recombination rate facilitates the separation of complex recombination processes into separate components.

We used two methods for the separation of complex recombination processes into residual ones, namely, graphical and analytical. The

graphical method is performed according to the following algorithm: We begin to apply the process of graphical separation in the field of low voltages. We draw a line ($R_{pr} = \text{const}$) parallel to the stress axis and subtract it from the experimental points of the reduced recombination rate. The result of the subtraction must be described by the function $\exp\left(\frac{eU}{2kT}\right)$. We change the position of the line ($R_{pr} = \text{const}$) until this happens. The line $R_{pr} = \text{const}$ is described by Eq. (5.4) for the first recombination center, which has the highest activation energy. The line $\exp\left(\frac{eU}{2kT}\right)$ is described by Eq. (5.3) for the second recombination center. We do the same for the next pair of recombination centers.

We find the characteristic points on the curves of the reduced recombination rate after we divide the experimental values of this quantity into components. The value of U_0 is the voltage at which the condition $R_{pr} = R_{pr}^{\max}/2$ then, $c_n n_1 + c_p P_1 = 2n_i \sqrt{c_n c_p} \exp\left(\frac{eU_0}{2kT}\right)$. We think that the energy level of the deep center is above the middle of the forbidden zone, $c_p p_1 < < c_n n_1$, then:

$$E_t = \frac{E_g - eU_0}{2} + \delta, \quad \text{where: } \delta = \frac{kT}{2e} \ln \left[\frac{1}{4} \frac{c_n N_c}{c_p N_v} \right] \quad (5.5)$$

The reduced recombination rate was calculated for various ratios of the capture coefficient of the capture coefficients and the result of the calculation is shown in Fig. 5. The correction is a value for silicon of about 0.01 eV and can be neglected. Different values of the capture coefficients introduce a certain systematic error. This value is equal to 0.06 eV for the calculations shown in Fig. 5. This error can be avoided, but for this it is necessary to measure the reduced recombination rate at several temperatures, as shown in Fig. 6. The temperature dependence of R_{pr} at a fixed bias voltage (U_1) is shown in Fig. 7.

The activation energy of the slope of a straight line (Fig. 7) is equal to:

$$E_a = 0.5E_g - E_t - eU_1 \quad (5.6)$$

Eq. (5.6) allows us to calculate the exact value of the activation energy of the recombination center. In our case, as expected, it is equal to the energy of the center at which the simulation was carried out, namely: 0.4 eV. Thus, the study of temperature dependences allows us to accurately estimate the activation energy.

We arrive at the following algorithm for determining the parameters of recombination centers with deep levels:

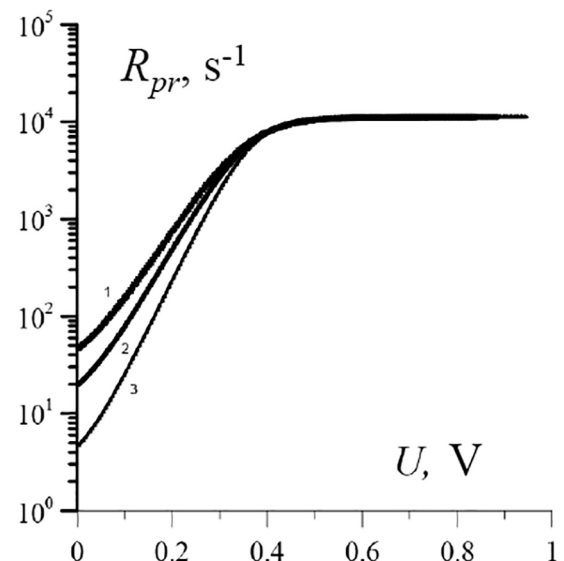


Fig. 6. Simulation of the reduced recombination rate of a deep center with an activation energy of 0.45 eV at different temperatures T , K: 1 – 350; 2 – 295; 3 – 220.

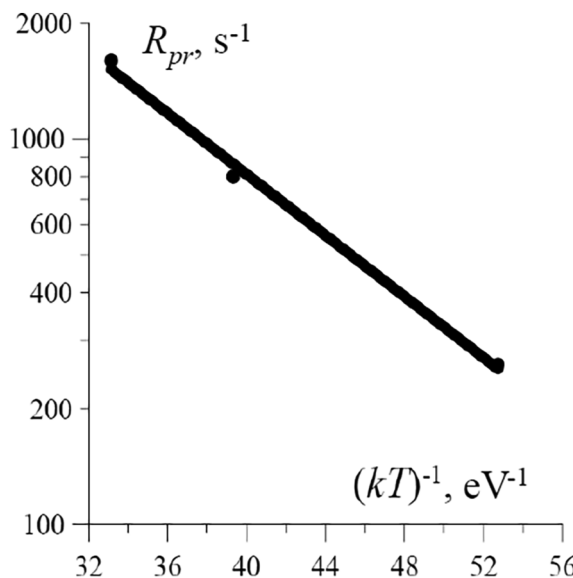


Fig. 7. Temperature dependence of the rate of reduced recombination at $U = 0.1$ V.

- We measure volt-ampere and volt-capacitive characteristics;
- We calculate the reduced recombination rate using Eq. (5.1);
- We divide recombination processes into components and find their characteristic parameters U_{oi} and $R_{np}^{\max} = \sqrt{c_n c_p} N_t / 2$:
- We estimate the activation energy with the help of Eq. (5.5) and specify it by the temperature dependence of the activation energy Eq. (5.6);
- We calculate c_p by Eq. (5.3) and the results of calculating the concentration of recombination centers using the TSC and DLTS method;
- We calculate c_n by Eq. (5.4) and the results of calculating the concentration of recombination centers using the TSC and DLTS method.

Lifetime in a highly doped n-type material (τ_{po}) and for a p-type (τ_{no}) can be calculated using formulas:

$$\tau_{po} = (c_p N_t)^{-1} = \frac{1}{2} \sqrt{\frac{c_n}{c_p}} (R_{np}^{\max})^{-1}, \quad \tau_{no} = (c_n N_t)^{-1} = \frac{1}{2} \sqrt{\frac{c_p}{c_n}} (R_{np}^{\max})^{-1} \quad (5.7)$$

We measured the forward current-voltage characteristics (Fig. 1) and calculated the reduced recombination rates for the diodes (Fig. 8). The parameters of the two recombination centers are presented in Table 2. These centers are responsible for the magnitude of the lifetime and the magnitude of the reverse currents.

The parameters of the centers can be calculated using other algorithms for the conversion of current-voltage characteristics using recombination spectroscopy methods: the derivative of the rate of reduced recombination, the differential slope of the current-voltage characteristic and its derivative with respect to the applied voltage. These techniques are described in [8-10]. All conversion algorithms produce the same results.

6. Temperature dependences of the deep-center capture coefficients

The current-voltage characteristics were measured in the range of 290–343 K.

The temperature dependences of the reduced recombination rate are shown in Fig. 9. The strong temperature dependence of the saturation region of a given value takes place. The separation of the

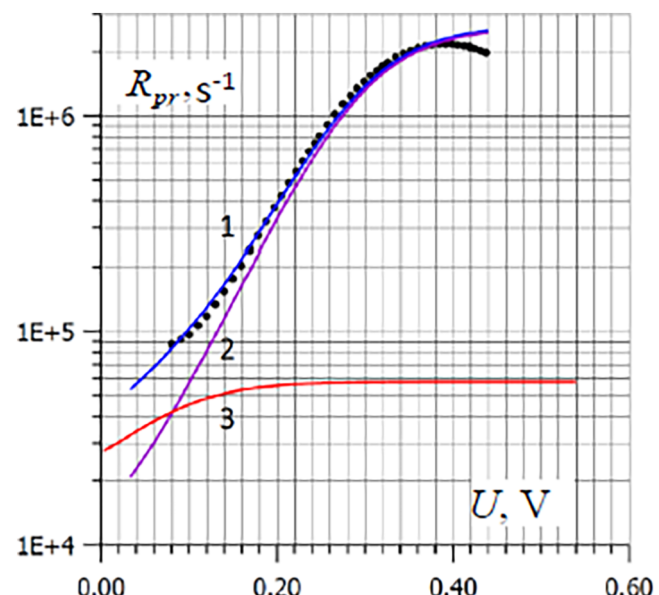


Fig. 8. Separation of the reduced recombination rate into components at $T = 294$ K. Points is the experiment; 1 – dependency restored by calculation; 2 – R_{pr} of 0.53 eV level; 3 – R_{pr} of 0.45 eV level.

Table 2
Parameters of deep centers.

No	$E_c - E_t$, eV	N_t , cm $^{-3}$	C_n , cm 3 s $^{-1}$	C_p , cm 3 s $^{-1}$	τ_{no} , s	τ_{po} , s
1	0.45	$3 * 10^{11}$	$3.8 * 10^{-5}$	$2.5 * 10^{-7}$	$2.6 * 10^{-8}$	$1.3 * 10^{-5}$
2	0.53	$4 * 10^{11}$	$6.0 * 10^{-5}$	$5.3 * 10^{-7}$	$4.2 * 10^{-8}$	$4.8 * 10^{-6}$

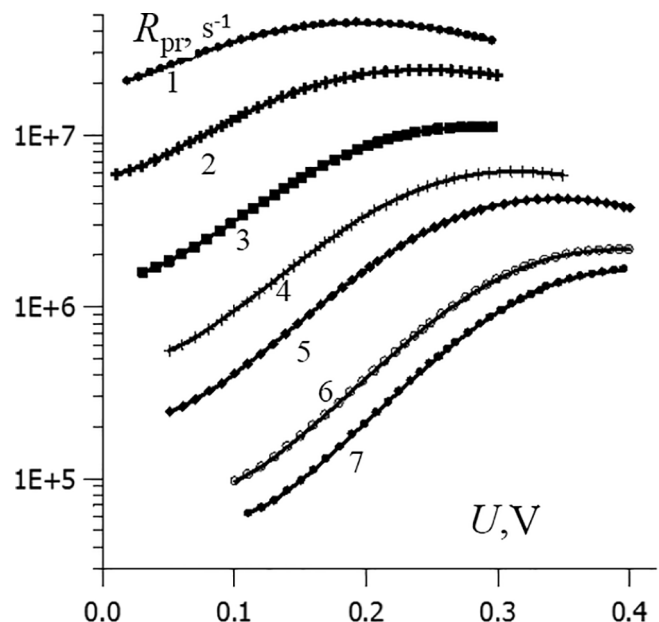


Fig. 9. Temperature dependence of the superficial recombination rate, T , K: 1 – 343; 2 – 333; 3 – 323; 4 – 313; 5 – 303; 6 – 294; 7 – 290.

reduced recombination rate into components was done for each temperature independently and the capture rate constant coefficients of holes and electrons for them were calculated. The results of the calculations are shown in Fig. 10 at the normal scale, and in Fig. 11 – semi-logarithmic. In addition, analytical approximations are defined for all capture rate constant coefficients in the form:

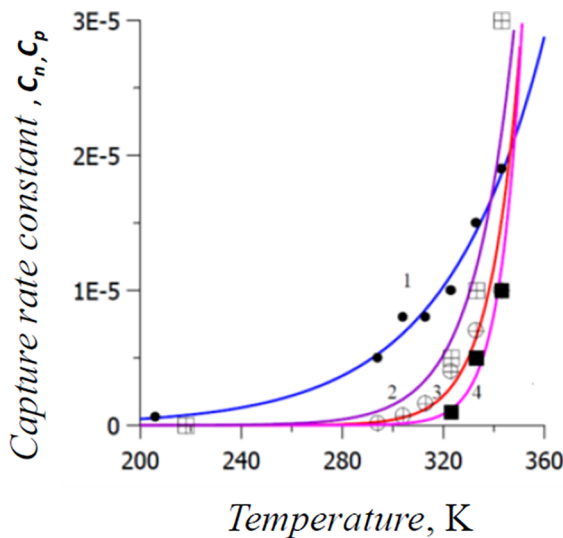


Fig. 10. Temperature dependences of the capture rate constant coefficients of deep centers with activation energies: 2, 4 – 0.53 eV; 1,3 – 0.45 eV. 1,2 – C_n ; 3,4 – C_p .

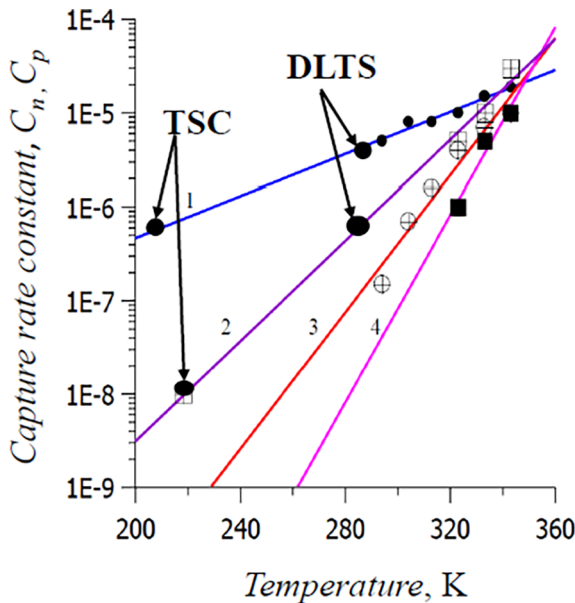


Fig. 11. Temperature dependences of the capture rate constant coefficients of deep centers with activation energies: 2, 4 – 0.53 eV; 1.3 – 0.45 eV. 1,2 – C_n ; 3,4 – C_p .

$$c_i = c_{0i} \exp\left(-\frac{E_{bi}}{kT}\right)$$

$$E_t = 0.53 \in B \left\{ \begin{array}{l} c_n = 8.6 \exp\left(-\frac{0.30}{kT}\right) \\ c_p = 1.9 * 10^8 \exp\left(-\frac{0.85}{kT}\right) \end{array} \right\}$$

$$E_t = 0.45 \in B \left\{ \begin{array}{l} c_n = 0.022 \exp\left(-\frac{0.16}{kT}\right) \\ c_p = 10^3 \exp\left(-\frac{0.57}{kT}\right) \end{array} \right\}$$

(6.1)

where E_{bi} is energy of nonradiative transition from excited to ground states.

The results of measuring the capture rate constant coefficients by various methods are consistent with each other. The capture rate constant coefficients, which were calculated from the TSC and DLTS experiments, are less than the results of calculations from the current-voltage characteristics. This fact is due to the strong temperature dependence of these coefficients and the fact that they were measured at different temperatures. The temperature at which these coefficients were calculated from TSC experiments is the lowest, so their value is the

smallest. The agreement of the results shows the correctness of the used models, experiments and calculations.

The results lead to the following conclusions:

1. Interpolation of the values of the electron capture rate constant coefficients for centers with energies of 0.45 and 0.53 eV, obtained from the temperature dependences of the current-voltage characteristics, coincides with the results of capacitive measurements using the methods of thermally stimulated capacitance and DLTS.
2. The strong temperature dependence of the capture rate constant coefficients speaks of the electron-phonon interaction during the ionization of deep centers and confirms the fact of the molecular nature of the centers in the form of complexes of silicon vacancies with impurity atoms. Such complexes have the form of a quasi-molecule in a matrix of crystalline silicon. These centers can have local phonons, which determine the electron-phonon interaction.

7. Calculation of the parameters of the electron-phonon interaction

The parameters of the electron-phonon interaction must be determined experimentally. In silicon, recombination centers are nonradiative and the optical method [21] cannot be used. In order to determine the parameters of nonradiative recombination centers, we use the configurational coordinate diagram of the recombination center shown in Fig. 12.

Configuration-coordinate diagram is a potential diagram of a deep center [25]. The potential energy of the center is plotted along the ordinate axis, and the generalized coordinate associated with the potential energy by simple relations is along the abscissa axis:

$$U_g = E_0 + 0.5\hbar\omega Q^2$$

$$U_u = E_0 + 0.5\hbar\omega (Q - Q_u + Q_g)^2,$$

(7.1)

where U_g , U_u are potential energies of the ground and excited states, $\hbar\omega$ is effective phonon energy; Q_g , Q_u are dimensionless generalized coordinates of the potential energy minima; E_0 is the energy distance between the minima of the potential energy. It is the energy of the purely electronic transition.

where U_u is adiabatic potential of the excited state; U_g is adiabatic potential of the ground state; E_0 is energy of a purely electronic transition from the conduction band to the level; E_b is energy of nonradiative transition from excited to ground state; E_{tj} is thermal emission activation energy.

To determine the parameters of the electron-phonon interaction, we use the characteristic energies of nonradiative transitions. This energy corresponds to the energy in the configuration diagram. It is associated with the parameters of the electron-phonon interaction as follows:

$$E_{Bi} = \frac{(E_0 - s\hbar\omega)^2}{4s\hbar\omega}$$

(7.2)

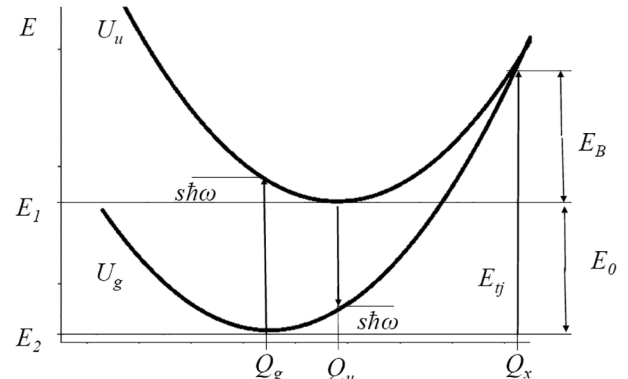


Fig. 12. Configuration-coordinate diagram of a defect in a crystal.

where s is the Huang and Rhys factor, which is equal to the number of phonons involved in the electron-vibrational transition; $s\hbar\omega$ is heat release in the theory of electron-phonon interaction. This value is equal to the energy that is transmitted to the lattice during the nonradiative capture of an electron or hole to a deep center.

We will take the energy that must be expended for the nonradiative ejection of an electron from a deep center as the second quantity to be calculated. These energies were determined experimentally from current-voltage characteristics and are 0.45 and 0.55 eV. In the configuration diagram, they correspond to the energy E_{ij} . In our notation, this value, and it is associated with the parameters of the electron-phonon interaction as follows:

$$E_{ij} = E_0 + E_B = \frac{(E_0 + s\hbar\omega)^2}{4 s\hbar\omega} \quad (7.3)$$

We get the desired parameters when we decide together (7.2) and (7.3):

$$\begin{aligned} s\hbar\omega &= (\sqrt{E_j} - \sqrt{E_B})^2 \\ E_0 &= (\sqrt{E_j} - \sqrt{E_B})(\sqrt{E_j} + \sqrt{E_B}) \end{aligned} \quad (7.4)$$

$$\sigma = \sqrt{2kT s \hbar\omega} \quad (7.5)$$

Thus, the strength of the electron-phonon interaction is mainly determined by heat generation and leads to an increase in the emission rate in an electric field.

The results of calculations and experiments performed on two recombination centers are summarized in Table 3.

Table 3 represents a complete set of parameters for two deep centers that allow one to calculate all the thermal, optical, and field dependences of deep centers.

8. The role of the electron-phonon interaction in the creation of reverse current-voltage characteristics of power diodes.

8.1. Reverse current

The space charge region of the device is depleted of free charge carriers at a reverse bias voltage, the equilibrium between recombination and generation is shifted towards generation. Reverse current is determined by the expression [2,11]:

$$I_{rev} = eS \int_0^w R dx \quad (8.1)$$

where R is the recombination rate; S is the diode area; w is the width of the depleted area.

The recombination rate must be found from a system of kinetic equations for the case of recombination with the participation of a doubly charged recombination center and under the condition $R = R_n = R_p$:

$$I_{rev} = eS \int_0^w \frac{e_n^t(x)e_p^t(x)N_t(x)}{e_n^t(x) + e_p^t(x)} dx \left\{ \begin{array}{l} e_n^t = r_n c_n N_c \exp(-(E_c - E_t)/kT) \\ e_p^t = r_p c_p N_v \exp(-(E_t - E_v)/kT) \end{array} \right\} \quad (8.2)$$

Table 3

Parameters of deep centers taking into account the electron-phonon interaction.

No	E_{nt} , eV	E_{pt} , eV	E_{no} , eV	E_{po} , eV	E_{Bn} , eV	E_{Bp} , eV
1	0.45	2.8	0.29	0.83	0.16	0.57
2	0.53	6.2	0.23	0.89	0.30	0.85
	$s\hbar\omega$, eV		N_b , cm^{-3}	C_{no} , $\text{cm}^3 \text{s}^{-1}$	C_{po} , $\text{cm}^3 \text{s}^{-1}$	σ , eV
1	0.073		$3 * 10^{11}$	0.022	1000	0.061
2	0.082		$4 * 10^{11}$	8.6	$1.9 * 10^8$	0.065

where r_n , r_p are factors of the degeneration of the level of the deep center for electrons and holes. Range of these factors is from 0.5 to 2; N_t is concentration of deep centers, n_t is electron concentration on them; e_n^t , e_p^t are emission rates of electrons and holes from deep centers; c_n , c_p are capture rate constants; E_t is recombination center energy; E_c , E_v are energies of the bottom of the conduction band and the ceiling of the valence band.

It should be noted that the rate of thermal emission depends on temperature exponentially; therefore, if the level of the recombination center recoils from the middle of the forbidden band by 3–5 kT, then, as a rule, the emission rate of electrons or holes is much greater than the rate of another transition. We obtain a simple expression for the reverse current of the diode:

$$I_{rev} = eSwN_t e_p^t \quad (8.3)$$

Thus, the reverse current is determined by the slowest emission process, which has an activation energy of more than half the band gap.

Expression (8.3) explains the temperature dependence of the reverse current, but does not explain the form of the current-voltage characteristic itself. The reverse current of power devices depends on the voltage. The type of current-voltage characteristic can be understood if we consider the influence of the electric field on the generation processes.

8.2. Poole-Frenkel's effect

Experimental results demonstrate an abnormally strong dependence of the current on the reverse voltage (Fig. 13a). Experimental data were subjected to transformation in order to identify the mechanisms that are responsible for the increase in current with increasing electrical voltage at the p-n-junction. We can make the following assumptions about this dependence. First, the height of the potential barrier surrounding the trap is reduced in the electric field, and the rate of carrier generation with its participation increases because there is a Poole-Frenkel effect (Fig. 13b) [12,13,19]. The influence of the Poole-Frenkel effect is confirmed by the linearity of the initial portion of the current-voltage characteristic, which was traced in the coordinates $\ln(I_{rev}) = f(\sqrt{F})$. Secondly, the rate of thermal emission is increased in the electric field due to the electron-phonon interaction. These factors lead to the fact that the reverse current increases with voltage faster than the Poole-Frenkel theory predicts. This is confirmed by the fact that the current-voltage characteristic is linear in the coordinates $\ln(I_{rev}) = f(F^2)$ [14,21].

The probability of generation of electrons and holes from defects increases in an electric field due to two main effects: the Poole-Frenkel effect, which is associated with a decrease in the activation energy of carrier ejection from a trap and acceleration of tunneling through defects. These phenomena will be considered sequentially.

The decrease in the activation energy of the trap, which is associated with the Poole-Frenkel effect is equal to [12,13,25]:

$$\Delta V = \frac{e^{3/2}}{\sqrt{\pi\epsilon_S}} \sqrt{F} = \beta_F \sqrt{F}; \quad \beta_F = \frac{e^{3/2}}{\sqrt{\pi\epsilon_S}} \quad (8.4)$$

where ϵ_S is a static dielectric constant, F is the electric field strength in the space charge region of the diode.

Thus, lowering the height of the potential barrier under the action of an electric field does not depend on the technological parameters of the diode. The multiplier before the root of the electric field of the expression (8.4) is called the Frenkel constant. Eqs. (8.3) and (8.4) allow us to calculate the expression for the p-n-junctions current-voltage characteristic at reverse bias:

$$I_{06p} = eSe_{p0}^t \int_0^W N_t(x) \exp\left(\frac{\beta_F \sqrt{F(x)}}{kT}\right) dx \quad (8.5)$$

where e_{p0}^t there is the rate of emission of holes without taking into account the influence of the electric field.

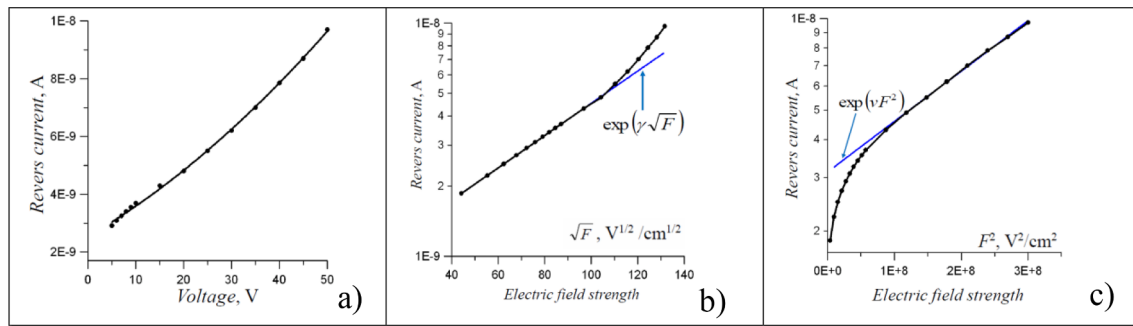


Fig. 13. Reverse current-voltage characteristics of the diodes. Point is experiment. F is the electric field strength in the space charge region of the device.

Poole-Frenkel's effect leads to the linearity of the volt-ampere characteristics in the coordinates $\ln(I_{rev}) = f(\sqrt{F})$, which is shown in Fig. 13b. The parameter β_F must be determined from the experimental current-voltage characteristics. Volt-ampere characteristic is a line in coordinates $\ln(I_{rev}) = f(\sqrt{F})$. Coefficient β_F is equal to the slope of this line. The result of the calculation should be compared with its value, which is calculated by the Eq. (8.4). The theoretical value of the Frenkel constant for silicon is $\beta_F/kT = 0.0088 \text{ V}^{-1/2} \text{ cm}^{1/2}$. The experimental value is more than 2 times. This is a consequence of the electron-phonon interaction. Value of the Frenkel constant for the electron-phonon interaction was calculated by Timashev [14]:

$$\gamma = \beta_F \left[1 + \frac{(E_{p0} - sh\omega)kT}{\sigma^2} \right] \quad (8.6)$$

Frenkel's constant must be more than 5 times in accordance with the Eq. (8.6) and Table 3. This value agrees qualitatively with the experiment, taking into account the errors of the theory, which relies on the one-coordinate model of the electron-phonon interaction.

The Timashev model has predicted that the rate of thermal emission grows faster in large fields compared to the Poole-Frenkel model [14]:

$$e_n^t = e_n^t(0) \exp(\gamma F^{1/2} + \lambda F^2) \quad (8.7)$$

The first term in the exponent describes the Poole-Frenkel effect, and the second additional increase in the rate of thermal emission in a strong electric field. Current-voltage characteristic should be linear in the coordinates $\ln(I_{rev}) = f(F^2)$, which is observed experimentally (Fig. 13c).

This result confirms the influence of the electron-phonon interaction, which accelerates the processes of emission in an electric field (Eq. (8.7)).

8.3. Quantum-mechanical calculation of the probability of an electronic-vibration transition from localized states of deep centers

The calculation of the probability of electronic transitions with the participation of deep centers must be performed taking into account the interaction of an electron or hole with lattice vibrations. Transitions between energy states are called electronic-vibration in this case.

There are two difficulties that are associated with the calculation of such transitions [31]. The first is related to the calculation of the wave functions of the electrons localized at the center. This is a difficult task. It is solved by applying model representations for the wave functions of the deep center. The second difficulty is associated with a lack of information about the nature of the electron-phonon interaction, which has a significant impact on the speed of electronic transitions.

These problems were overcome in [31]. The expression for the probability of a quantum-mechanical transition, taking into account the electron-phonon interaction, can be written in the form in accordance with this application:

$$W = \sum_{i,j} \int_{-\infty}^{\infty} W_{0i,j}(E_{t,i,j} - \varepsilon) f_{i,j}(\varepsilon) d\varepsilon \quad (8.8)$$

where $W_{0i,j}(E_{t,i,j} - \varepsilon)$ is a probability of a purely electronic transition from the i -sublevel of the multiplet of the initial state of the center to the j -sublevel of the final state of the multiplet; $f_{i,j}(\varepsilon)$ is an expression for the form-function of the electronic-vibration transition from i -the sublevel of the initial state of the center to j -the sublevel of the final state of the multiplet; $\sum_{i,j}$ is a sum over all sublevels of multiplets 1 and 2.

Eq. (8.8) is written for a situation where the energy spectrum consists of two groups of close levels (1_i ; 2_j) separated by a large energy gap. Let the electron transition be between singlet states, then:

$$W_{n,p}(F, T) = \int_{-\infty}^{\infty} W_{0n,p}(E_{t,n,p} - \varepsilon) f_{n,p}(\varepsilon) d\varepsilon \quad (8.9)$$

Eq. (8.9) is a generalized expression for the probability of an electronic transition, which allows us to calculate the dependences of the probabilities of electronic-vibration transitions on the electric field strength and temperature and not use the single-coordinate model. Such an approach makes it possible to avoid simplifying the complex interaction of electrons with a lattice. This expression can be used for multiphonon thermal, tunnel, and optical transitions. Eq. (8.9) can be used when the formula of a purely electronic transition is the formula that expresses this mechanism. In the first approximation, we consider that a purely electronic transition is a tunnel one, and the Gauss function is the form-function of the electronic-vibration transition. The probability of a tunnel junction for tunneling through a potential triangular barrier has the form [31]:

$$W_{0n}(E_{tii} - \varepsilon) = \frac{eF}{\sqrt[3]{2m^*(E_{tn} - \varepsilon)}} \exp\left(\frac{4(E_{tn} - \varepsilon)^{3/2}\sqrt{m^*}}{3heF}\right) \quad (8.10)$$

where $E_{tn,p}$ is the energy of a purely electronic transition from the deep level to the conduction band or the valence band; F is the electric field strength; $f_{n,p}(\varepsilon)$ is a form-function of an electronic-vibration transition. The form-function is:

$$f_{n,p}(\varepsilon) = \frac{1}{\sigma\sqrt{2\pi}} \exp\left(-\frac{(\varepsilon - E_{tn,p})^2}{2\sigma^2}\right) \quad (8.11)$$

The transition probability Eq. (8.9) is equal to the thermal emission rate in Eq. (8.3), and then the expression for the reverse current of the diode is:

$$I_{rev} = eSwN_t W_{n,p}(F, T) \quad (8.12)$$

The magnitude of the reverse current of the diode was calculated from Eq. (8.12), taking into account Eqs. (8.9)–(8.11), as well as the data presented in Table 3. Moreover, we take into account the parameters of transition of holes from the valence band to the level of a recombination center with an energy of 0.53 eV, since this center is located near the middle of the silicon band gap. The calculation results are compared with the experiment in Fig. 13a. The results of the calculation and experiment are in agreement between themselves, which

proves the calculations are correct.

9. Conclusions

The calculations and experiments that were performed in this article show the drawbacks of simple classical formulas for describing recombination and generation processes in semiconductor p-n-junctions. The ideality factor is not constant and depends on the recombination fluxes of electrons and holes, which change as a result of injection. Algorithms for converting current-voltage characteristics are taking place. These algorithms allow one to estimate the parameters of the recombination centers when the temperature of the experiment does not change. Processing current-voltage characteristics together with measurements of the capacitance of p-n-junctions allow us to calculate a large set of parameters of the recombination centers, including the parameters of the electron-phonon interaction. The electron-phonon interaction leads to the fact that the reverse current of p-n-junctions increases with increasing voltage faster, which is predicted by the Poole-Frenkel theory. This is proved by the calculations and experiments that are carried out in this article. General considerations of a physical nature suggest that the electron-phonon interaction should be stronger when the recombination centers are molecules of the type of complexes of a vacancy with an impurity. Such centers may be weakly associated with the main lattice, and in this case the vibrations of the main lattice less suppress the molecular vibrations inside such centers.

The work is supported by the grant 0004-2019-0002.

References

- [1] Shockley W. The theory of p-n-Junction in semiconductor and p-n-Junction transistors. *Bell Syst Tech* 1949;28:435.
- [2] Sah CT, Noyce RN, Shockley W. Carrier generation and recombination in p-n junctions and p-n junction characteristics. *Proc IRE* 1957;45(9):1228–43.
- [3] Eremenko VG, Nikitenko VI, Yakimov EB. Investigation of the nature of the diode effect on dislocations in silicon. *Sov Phys JETP* 1975;40(3):570–6.
- [4] Kimoto T, Takemura O, Matsunami H, Nakata T, Inoue M. Al + and B + implantations into 6H-SiC epilayers and application to p-n Junction diodes. *J Electron Mater* 1998;27(4):358–64.
- [5] Al Abdullah K, Al Alloush F, Jaafar Ali, Salame C. Study of the effects related to the electric reverse stress currents on the Mono-Si solar cell electrical parameters. *Energy Procedia* 2013;36:104–13.
- [6] Xiong Zou Xu, Zhang Xing Lu, Tang Chak Wah, Lau Kei May. Fully-vertical GaN p-i-n diodes using GaN – on – Si epilayers. *IEEE Electron Device Lett* 2015. <https://doi.org/10.1109/LED.2016.2548488>.
- [7] Inoue N, Itoh A, Kimoto T, Matsumoto H. Hot-Implantation of nitrogen donors into p-type α -SiC and characterization of n-p-junction. *J Electron Mater* 1997;26(3):165–71.
- [8] Bulyarskiy SV, Grushko NS, Somov AI, Lakalin AV. Recombination in the space charge region and its effect on the transmittance of bipolar transistors. *Semiconductors* 1997;31(9).
- [9] Bulyarskiy SV, Grushko NS, Lakalin AV. Differential methods for determination of deep-level parameters from recombination currents of p-n junctions. *Semiconductors* 1998;32(10).
- [10] Bulyarskiy SV, Vorob'ev MO, Grushko NS, Lakalin AV. Deep-level recombination spectroscopy in GaP light-emitting diodes. *Semiconductors* 1999;33(6).
- [11] Sze SM. Physics of Semiconductor Devices. New York: John Wiley & Sons; 1981. p. 455.
- [12] Shan Q, Meyya DS, Cho QD, Schubert EF, Son JK, Sone Ch. Transport-mechanism analysis of the reverse leakage current in GaInN light-emitting diodes. *Appl Phys Lett* 2011;99:253506.
- [13] Musolino M, van Treeck D, Tahraoui A, Scarparo L, De Santi C, Meneghini M, Zanoni E, Geelhaar L, Riechert H. A physical model for the reverse leakage current in (In, Ga)N/GaN light-emitting diodes based on nanowires. *J Appl Phys* 2016;119:044502.
- [14] Timashev SF. On the Frenkel effect during thermofield ionization of deep centers in the space charge layer in semiconductors. *Phys Solid State* 1974;16:804–11.
- [15] Obreja VVN. On the leakage current of present-day manufactured semiconductor junctions. *Solid-State Electron* 2000;49(1):49–57.
- [16] Sukach AV, Tetyorkin VV, Tkachuk AI. Carrier transport mechanisms in reverse biased InSb p-n junctions. *Semicond Phys Quantum Electr Optoelectr* 2015;18(3):267–71. <https://doi.org/10.15407/spqeo18.03.267>.
- [17] Huang Kuan-Chih, Dahal R, Lua JJ-Q, Danon Y, Bhat IB. Continuous p-n junction with extremely low leakage current for microstructured solid-state neutron detector applications. *Proc SPIE* 2013;8710. <https://doi.org/10.1117/12.2016121>.
- [18] Bouangeune D, Lee Ye-Ji, Ho Cho D, Shim KH, Choi Ch J. Reverse current conduction mechanism of transient voltage suppression diode under electrostatic discharge stress. *Mater Trans* 2014;55(11):1733–7. <https://doi.org/10.2320/matertrans.M2014214>.
- [19] Obreja VVN, Obreja AC. Bulk and edge (surface) leakage reverse current in p-n junctions from commercial semiconductor devices. IEEE; 2009.
- [20] Vinogradov VS. Multiphonon light absorption theory. *Phys Solid State* 1970;12:3081–91.
- [21] Bulyarskiy SV, Grushko NS, Gudkin AA. Field dependences of thermal ionization of deep centers in the space charge layer of Au – n-InP: Fe barriers. *Semiconductors* 1975;9:287–91.
- [22] Makram-Ebeid S. Effect of electric field on deep-level transients in GaAs and GaP. *Appl Phys Lett* 1980;37(5):464–70.
- [23] Makram-Ebeid S, Lannoo M. Quantum model for phonon assisted tunnel ionization of deep levels in semiconductors. *Phys Rev* 1982;25(10):1082–90.
- [24] Perel Karpus VI. Multiphonon ionization of deep centers in semiconductors in an electric field. *J Exp Theoretical Phys* 1986;64:1376–91.
- [25] Ridley B. Quantum Processes in Semiconductors. 2nd ed. Oxford: Clarendon Press; 1988.
- [26] Sah CM, Forbes A. Thermal and optical emission and cross section of electrons and holes at imperfection centers in semiconductors from photo dark junction current capacitance experiment. *Sol State Electron* 1970;13:758–769.
- [27] Bulyarskiy SV, Radautsas SI. Determination of the parameters of deep recombination centers using a modified thermally stimulated capacitance method. American Institute of Physics, 1063–7826/81/15. *Semiconductors* 1981;15:1443–6.
- [28] Bulyarskiy SV, Grushko NS. Thermally stimulated current and capacitance of spatial charge regions containing multiply charged impurity centers. American Institute of Physics, 1063–7826/87/21. *Semiconductors* 1987;21:1730–2.
- [29] Lang DV. Fast capacitance transient apparatus: application ZnO and O centers in GaP p-n-junction/. *J Appl Phys* 1974;45:1730–6.
- [30] Shockley W, Read WT. Statistics of the recombination of holes and electrons. *Phys Rev* 1952;87:835–42.
- [31] Bulyarskiy SV, Grushko NS, Zhukov AV. Calculation of the field dependence of the rates of emission of carriers from deep centers based on an experimental form-function for the optical transition. *J Exp Theor Phys* 1999;89(3):547–51.

Further Reading

- [1] Bulyarskiy SV, Lakalin AV, Abanin IE, Amelichev VV, Svetuhin VV. Optimization of the parameters of power sources excited by β -radiation. *Semiconductors* 2017;51(1):66–72.
- [2] Saurov AN, Bulyarskiy SV, Risovaniy VD, Shamaeva AA, Lebedeva EA. Nanostructured current sources based on carbon nanotubes excited by β radiation. *Semiconductors* 2016;50(13):1744–7.
- [3] Bulyarskiy SV, Ionychev VK, Kuz'min VV. Tunneling recombination in silicon avalanche diodes. *Semiconductors* 2003;37(1):115–8.
- [4] Bulyarskiy SV, Zhukov AV, Zyuzin AM, Prikhod'ko VV. Calculation of the shape of the R line of the Mn4+ ion in gadolinium-gallium garnet. *J Exp Theor Phys* 2002;95(6):1085–91.
- [5] Bulyarskiy SV, Grushko NS, Zhukov AV. Calculation of the probability of nonradiative electronic transitions from deep centers in GaAs in the one-coordinate approximation. *Opt Spectr (English translation of Optika i Spektroskopiya)* 2001;90(3):381–6.
- [6] Bulyarskiy SV, Grushko NS, Zhukov AV. Calculation of the probability of nonradiative electronic transitions from deep centers in GaAs in the one-coordinate approximation. *Opt Spektrosk* 2001;90(3):440–5.
- [7] Bulyarskiy SV, Vorob'ev MO, Grushko NS, Lakalin AV. Deep-level recombination spectroscopy in GaP light-emitting diodes. *Semiconductors* 1999;33(6):668–71.
- [8] Bulyarskiy SV, Grushko NS, Lakalin AV. Differential methods for determination of deep-level parameters from recombination currents of p-n junctions. *Semiconductors* 1998;32(10):1065–8.
- [9] Bulyarskiy SV, Grushko NS, Lakalin AV. Two methods for determining the activation energy of deep levels from an analysis of the recombination current in the space-charge region of a p - n junction. *Indust Lab* 1997;63(7):408–13.
- [10] Bulyarskiy SV, Grushko NS, Somov AI, Lakalin AV. Recombination in the space charge region and its effect on the transmittance of bipolar transistors. *Semiconductors* 1997;31(9):983–7.
- [11] Bulyarskiy SV, Butylkina NA, Grushko NS, Nazarov MV, Stepin IO. Inhomogeneities in silicon p-n-junctions. *Soviet Phys J* 1991;34(4):339–42.



Sergey Viktorovich Bulyarskiy, Professor, Doctor of Science, Corresponding Member of Tatarstan Academy of Sciences (Russia), Principal Research Scientist in Institute of Nanotechnology of Microelectronics of the Russian Academy of Sciences (Moscow, Russia), author of more than 600 scientific articles (including 23 monographs). Scientific research areas: thermodynamics in nanotechnology; transport phenomena in nano- and microelectronic structures.